Biosensors and Bioelectronics 26 (2010) 964–969

Contents lists available at ScienceDirect

Biosensors and Bioelectronics

journal homepage: www.elsevier.com/locate/bios

Label free detection of white spot syndrome virus using lead magnesium niobate–lead titanate piezoelectric microcantilever sensors

Joseph A. Capobianco [a], Wei-Heng Shih [a], Jiann-Horng Leu [b,1], Grace Chu-Fang Lo [b], Wan Y. Shih [c,*]

[a] Department of Materials Science and Engineering, Drexel University, Philadelphia, PA 19104, United States
[b] College of Life Science, National Taiwan University, Taipei, Taiwan
[c] School of Biomedical Engineering, Science, and Health Systems, Drexel University, Philadelphia, PA 19104, United States

ARTICLE INFO

Article history:
Received 19 April 2010
Received in revised form 17 July 2010
Accepted 2 August 2010
Available online 11 August 2010

Keywords:
Virus
Detection
Piezoelectric
Cantilever
Sensor
Detection

ABSTRACT

We have investigated rapid, label free detection of white spot syndrome virus (WSSV) using the first longitudinal extension resonance peak of five lead–magnesium niobate–lead titanate (PMN–PT) piezoelectric microcantilever sensors (PEMS) 1050–700 μm long and 850–485 μm wide constructed from 8 μm thick PMN–PT freestanding films. The PMN–PT PEMS were encapsulated with a 3-mercaptopropyltrimethoxysilane (MPS) insulation layer and further coated with anti-VP28 and anti-VP664 antibodies to target the WSSV virions and nucleocapsids, respectively. By inserting the antibody coated PEMS in a flowing virion or nucleocapsid suspension, label free detection of the virions and nucleocapsids were respectively achieved by monitoring the PEMS resonance frequency shift. We showed that positive label free detection of both the virion and the nucleocapsid could be achieved at a concentration of 100 virions (nucleocapsids)/ml or 10 virions (nucleocapsids)/100 μl, comparable to the detection sensitivity of polymerase chain reaction (PCR). However, in contrast to PCR, PEMS detection was label free, in situ and rapid (less than 30 min), potentially requiring minimal or no sample preparation.

1. Introduction

White spot syndrome virus (WSSV) is a devastating shrimp viral pathogen that causes serious economic losses to shrimp aquaculture industry globally. This virus has a wide host range, attacking shrimp, crabs, lobster as well as many other crustaceans (Corbel et al., 2001; Wang et al., 1998; Lo et al., 1996a; Flegel, 2006), but the penaeid shrimp are most vulnerable to WSSV infection. In shrimp farms, WSSV infection causes up to 100% mortality within three to ten days following the first signs of infection (Lightner, 1996). These clinical signs include a sudden reduction in food consumption, lethargy, loose cuticle, reddish discoloration, and the presence of white spots in the shrimp cuticle (Chou et al., 1995; Wang et al., 1995; Lightner, 1996). Diagnosis for WSSV infection based on the gross signs of diseased shrimp is not practical for shrimp farming practices, as these clinical signs are not the pathonognomic characters only specific to WSSV infection, and the shrimp exhibiting these signs are at late stage of WSSV infection, indicating the outbreak of disease has occurred and preventive measures are too late. Therefore, it is necessary to develop a diagnostic method that can detect WSSV at low level or at early stage of infection. Various WSSV diagnostic methods have been developed, including polymerase chain reaction (PCR) (Takahashi et al., 1996; Lo et al., 1996a,b; Kimura et al., 1996), in situ hybridization (Durand et al., 1996; Chang et al., 1996; Wongteerasupaya et al., 1996), histological observation of sectioned tissue (Wongteerasupaya et al., 1995; Wang et al., 1997), and immunological-based methods (Poulos et al., 2001; Anil et al., 2002; Liu et al., 2002).

Currently, PCR is the most widely used method for WSSV detection, as it provides high specificity and sensitivity. Most of the commercial kits for WSSV diagnosis are based on this technology, and many different protocols have been developed. The Taqman real-time PCR was the most sensitive method, which could detect WSSV of 4–5 copies per reaction (Durand and Lightner, 2002; Sritunyalucksana et al., 2006). The nested two-step PCR methods detected 50–100 copies of WSSV, whereas the one-step PCR could detect 1000 copies (Sritunyalucksana et al., 2006). Immunological-based diagnostic methods have been investigated or developed including immunodot test (Anil et al., 2002) and antigen-capture ELISA (Ac-ELISA) test (Liu et al., 2002). Their detection limits are about 400–500 pg of WSSV protein, and are comparable to one-step PCR. The immunological-based kit using lateral flow chromatographical detection strips is now commercially available (Shrimple

* Corresponding author. Tel.: +1 3258952325.
E-mail address: shihwy@drexel.edu (W.Y. Shih).
[1] Current address: Center for Marine Bioenvironment and Biotechnology, National Taiwan Ocean University, No. 2, Pei-Ning Road, Keelung 20224, Taiwan, ROC.

0956-5663/$ – see front matter © 2010 Elsevier B.V. All rights reserved.
doi:10.1016/j.bios.2010.08.004

Test Kits). The sensitivity is not high (>10,000 viral particles), but the kit is cheap, easy to use, and do not need the use of specific instrument. Therefore, it is suitable for use at pond-side by farmers to verify disease outbreaks. Although the sensitivity of immunological-based detection method can only reach the limit of one-step PCR, the sample preparation processes for immunological detection is simple, time-saving and without the need of expensive instruments. Therefore, techniques based on antibody–antigen reaction are still continuously developed for WSSV detection; for example, the reverse passive latex agglutination assay (Okumura et al., 2005) and surface plasmon resonance (SPR) techniques (Lei et al., 2008).

Piezoelectric microcantilever sensors (PEMS) are a new type of sensors that consist of a highly piezoelectric layer such as lead zirconate titanate (PZT) or lead–magnesium niobate–lead titanate $(PbMg_{1/3}Nb_{2/3}O_3)_{0.63}$–$(PbTiO_3)_{0.37}$ (PMN–PT) (Shih et al., 2006) bonded to a non-piezoelectric layer such as glass, tin, or copper. Receptors or antibodies specific to target molecules can be immobilized on the PEMS surface. Binding of target molecules to the PEMS surface shifts the PEMS resonance frequency. Real-time, in situ, label free detection of the target molecules can be achieved by monitoring the PEMS resonance frequency shift using simple electrical means. Compared to silicon microcantilevers, PEMS do not require complex optical components, and their quality factor which is defined as the ratio of the peak frequency over the width at half the peak height can remain high when submerged in a liquid medium (Yi et al., 2003). PEMS can be electrically insulated using a silane base coating (Capobianco et al., 2006, 2007, 2008) or paralyene (Hwang et al., 2004) for in-liquid detection. PEMS have successfully been used in rapid, label free, and sensitive detection of bacteria (Capobianco et al., 2006; Zhu et al., 2007a,b) in phosphate buffer saline solution (PBS), human epidermal growth factor receptor 2 (Her2) in PBS with a background of bovine serum albumin (BSA) (Capobianco et al., 2007, 2008), and spores in PBS and in water (McGovern et al., 2007, 2008).

Although PEMS use electrical means for detection and silicon microcantilevers use optical means or piezoresistivity for detection, PEMS resonator sensors (Yi et al., 2002) and silicon microcantilever (Chen et al., 1995)/silicon nanocantilever (Gupta et al., 2006) resonator sensors have long been regarded as the same type of sensors in that (1) both use flexural mode resonance peaks for detection and (2) both are mass sensors, i.e., binding of target antigen to the receptors on the sensor surface increases the sensor mass that in turn decreases the sensor resonance frequency. Interestingly, our recent studies and others' on PZT PEMS showed that PZT PEMS detection resonance frequency shift was more than 100-times larger than could be accounted for by the mass change (Lee et al., 2004a,b, 2005; Shen et al., 2006; Zhu et al., 2007a,b). These results clearly set PEMS apart from mass sensors. In addition, highly piezoelectric materials such as PMN–PT are prone to polarization orientation change under stress or under an electric field. Studies on PMN–PT PEMS showed that the flexural mode detection resonance frequency shift of PMN–PT PEMS was a result of the elastic modulus change due to the stress-induced polarization orientation change in the PMN–PT layer by the binding of the target analyte to the PEMS surface (Zhu et al., 2008a,b; Shih et al., 2008). Due to this elastic modulus change mechanism, the detection sensitivity of a PMN–PT PEMS was amplified 300 times (Zhu et al., 2008a,b; Shih et al., 2008) higher than could be accounted for by mass loading alone. Zhu et al. (2008a,b) further showed that PMN–PT PEMS could also exhibit high-frequency non-flexural resonance modes such as longitudinal extension modes that non-piezoelectric microcantilevers such as silicon-based microcantilevers lack as a result of the high piezoelectricity of the piezoelectric layer. In view of a PMN–PT PEMS amplified detection resonance frequency shift through its elastic modulus change mechanism and that it also offers higher frequency non-flexural mode resonance peaks, it is of interest to investigate PMN–PT PEMS for WSSV detection.

The purpose of this study is to investigate the label free detection of WSSV using the first longitudinal mode resonance peak of a PMN–PT PEMS consisted of 8 μm thick PMN–PT freestanding sheet bonded with a 2 μm thick copper layer that exhibits elastic modulus change induced detection enhancement. We carried out direct detection of virions and the nucleocapsides by targeting an envelope protein, VP28 and the nucleocapsid protein, VP664, respectively. For comparison we also removed the envelope of the viruses and detected the isolated nucleocapsids by targeting the nucleocapsid protein VP664.

2. Experimental

2.1. PMN–PT PEMS fabrication

Five PMN–PT/Cu PEMS were used in this study. They were constructed from PMN–PT freestanding sheets of 8 μm in thickness. A 150 nm thick gold layer with a 15–30 nm thick chromium bonding layer was first deposited on one side of the PMN–PT freestanding sheet by evaporation (E-gun Evaporator, Semicore Equipment, Livermore, CA) to serve as an electrode for plating. A 2 μm thick copper layer was electroplated on the gold surface at a rate of 500 nm/min as the non-piezoelectric layer using a plating solution of copper sulfate. After copper plating, a 150 nm thick gold was evaporated on both sides of the sheet. The PMN–PT/Cu bilayer was then embedded in wax and cut to the cantilever shape with a wire saw (Princeton Scientific Precision, Princeton, NJ). After attaching the wires to the top and bottom electrodes using conductive glue (XCE 3104XL, Emerson and Cuming Company, Billerica, MA), the PMN–PT/Cu strips were finally glued to a glass substrate to form the microcantilevers (Shih et al., 2006; Zhu et al., 2008a,b).

2.2. Electrical insulation of PEMS

The PEMS was first soaked in a diluted (1:100 in water) piranha solution (two parts of 98% sulfuric acid (Fisher, Fair Lawn, NJ) with one part of 30% hydrogen peroxide (FisherBiotech, Fair Lawn, NJ)) at 20 °C for 1 min to clean the gold surfaces. The PEMS was then submerged in 0.1 mM solution of 3-mercaptopropyltrimethoxysilane (MPS) in ethanol (Tremont et al., 2000) covered with parafilm to prevent ethanol evaporation for 30 min. The PEMS was then dried in a vacuum-oven (Model 1400E, VWR International) at 762 mm Hg overnight followed by soaking in a 1 vol.% MPS solution in ethanol titrated to a pH 4.5 with acetic acid and covered with parafilm for 36 h with the solution being changed every 12 h. They then dried overnight in a vacuum-oven (Model 1400E, VWR International) at 762 mm Hg and rinsed with ethanol. Based upon our previous results we estimated the thickness of the MPS layer to be about 250 nm (Capobianco et al., 2007, 2008).

2.3. Purifications of WSSV virions and nucleocapsids

The WSSV in this study was originated from WSSV-infected *P. monodon* collected in Taiwan in 1994 (Wang et al., 1995; GenBank accession number AF440570), and then propagated in specific pathogen-free *L. vannamei* to prepare the virus stock (Wang et al., 2007). The inocula were prepared from the stock and injected into healthy crayfish *P. clarkii* according to Tsai et al. (2004). At one week post infection, the moribund crayfish were collected and the virions were purified from the crayfish tissues according to the methods developed by Xie et al. (2005). The OD_{600} value of purified WSSV virions was determined by using a spectrophotometer

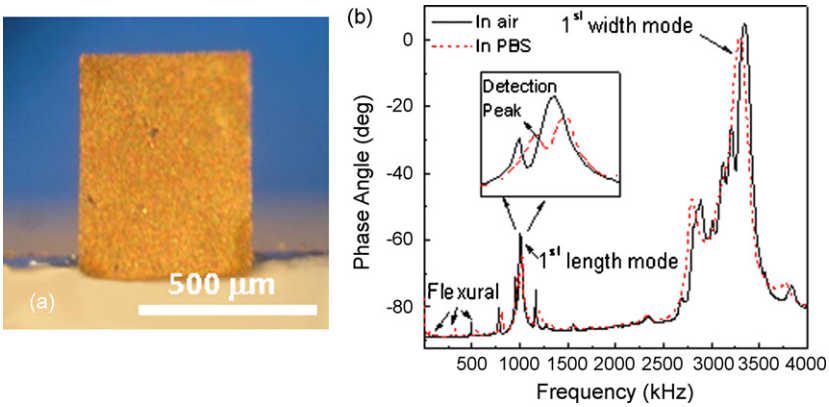

Fig. 1. (a) An optical micrograph of a 715 μm long and 485 μm wide PMN–PT PEMS viewed from the gold side and (b) a typical phase angle versus frequency resonance spectra of a PMN–PT PEMS in air and in PBS. The detection was carried out with the first longitudinal peak.

and the concentration of the corresponding virions was then calculated using the formula established by Zhou et al. (2007). To purify the WSSV nucleocapsids, a known amount of purified WSSV virions were treated with 1% Triton X-100 in TMN buffer (20 mM Tris–HCl, 150 mM NaCl, 2 mM $MgCl_2$, pH 7.5) for 30 min at room temperature with occasional shaking. Subsequently, the samples were centrifuged at 20,000 × *g* for 20 min at 4 °C, rinsed with water and then resuspended with TMN buffer. We assumed that the amount of purified nucleocapsids equal to that of the input virions.

2.4. Antibody purification

Polyclonal anti-VP28 and anti-VP664 antibodies were raised by injecting recombinant VP28 and VP664 in rabbits. After collecting the sera from the rabbits, ImmunoPure (Protein A) IgG Purification Kit (Pierce Biotechnology) was used to purify the anti-VP28 and anti-VP664 antibodies from the corresponding rabbit antisera according to the supplier's protocol. The purified antibodies were desalted and concentrated in phosphate-buffered saline through an Amicon Ultra-15 centrifugal filter device (Millipore). Subsequently, the antibodies were quantified using the Bradford method (BioRad), and freeze-dried for long term storage until use.

2.5. Antibody immobilization

A heterobifunctional crosslinker, sulfosuccinimidyl 4-N-maleimidomethyl cyclohexane-1-carboxylate (sulfo-SMCC) was used to tether the purified VP28 or VP664 antibodies to the PEMS surface. The antibody was first covalently bonded to sulfo-SMCC by using 1 ml solution containing 1 μM antibody and 80 μM sulfo-SMCC for 2 h at 4 °C for the NHS-ester of the sulfo-SMCC to react with a primary amine of the antibody to form a peptide bond. Unreacted sulfo-SMCC molecules were then removed by repeated microcentrifugation at 6000 RPM with a 10 kD filter (Millipore) three times. The MPS-coated PEMS was then soaked in the sulfo-SMCC-linked antibody solution with 5 mM ethylenediaminetetraacetic acid (EDTA) (Pierce) for 2 h to immobilize the antibody on the MPS coating surface via the reaction of the maleimide of the sulfo-SMCC with the sulfhydryl of the MPS. Following the antibody immobilization the PEMS was submerged in a 30 mg/ml BSA solution in PBS for non-specific binding prevention (Capobianco et al., 2007, 2008). At this point, the PEMS may be stored in a humidified container in a refrigerator for up to several days before being used for detection. A total of 5 PEMS were used throughout this study.

3. Results and discussions

3.1. PEMS resonance spectra

Fig. 1(a) shows an optical micrograph of a PEMS 715 μm long and 485 μm wide viewed from the gold side. For a PEMS with a thickness *h*, length *L*, and a sound velocity *c*, the first longitudinal extension mode is $c/4L$ (Capobianco, 2009). On the other hand, the resonance frequency of a flexural mode is proportional to ch/L^2 (Yi et al., 2002). Therefore, the resonance frequency of a longitudinal mode could be higher than that of a flexural mode by a factor on the order of the aspect ratio, L/h. For a PEMS 715 μm long and 10 μm thick (8 μm PMN–PT and 2 μm copper), L/h was about 71. We show the typical PEMS phase angle versus frequency resonance spectra in Fig. 1(b). The dashed and solid lines represent the spectra in air and in PBS, respectively. As can be seen, the first longitudinal peak was at around 1000 kHz, which was much higher than the flexural peaks as marked by arrows. In addition, the longitudinal peak can better withstand liquid damping than flexural modes. As can be seen in Fig. 1(b), the first longitudinal extension mode retained much of the peak height with a *Q* value of about 25 in PBS.

3.2. Flow system and WSSV detection

For detection, the PEMS were vertically inserted in the center of a home-made polycarbonate flow channel with its major faces parallel to the flow as shown in the photograph in Fig. 2(a) and the schematic in Fig. 2(b). The detection chamber was 18.5 mm long, 3.5 mm wide, and 5.5 mm deep (volume = 356 μl) driven with a peristaltic pump (model 77120-62, Cole-Parmer's Master Flex, Vernon Hills, IL). All experiments were carried out at a flow rate of 1 ml/min corresponding to an average flow velocity of 1.4 mm/s. A stock virus (nucleocapsid) suspension (10^9 virus/ml) was diluted to suspensions of 10^8–50 viruses/ml using 1:10 serial dilution. Before each detection, we first flowed PBS to allow the PEMS to equilibrate with the PBS at room temperature until the resonance frequency of the PEMS become stable, i.e., with no more than 100 Hz shift in 30 min. A similar stabilization procedure has been employed in other resonator detection systems (Sakti et al., 1999). Once the PEMS had stabilized, 10 min of background monitoring was performed for $t = -10$ to 0 min. At $t = 0$ min, 60 μl of a concentrated suspension of viruses or nucleocapsids in PBS was spiked in the reservoir (see Fig. 2(a)). A total liquid volume of 6 ml was used, most of which resided in the reservoir and the long tubes connecting the detection chamber and the reservoir. Injecting 60 μl of a suspension of 1×10^7–5×10^3 viruses/ml in the reservoir yielded concentrations of 10^5–50 virions (nucleocapsids)/ml in the flow system.

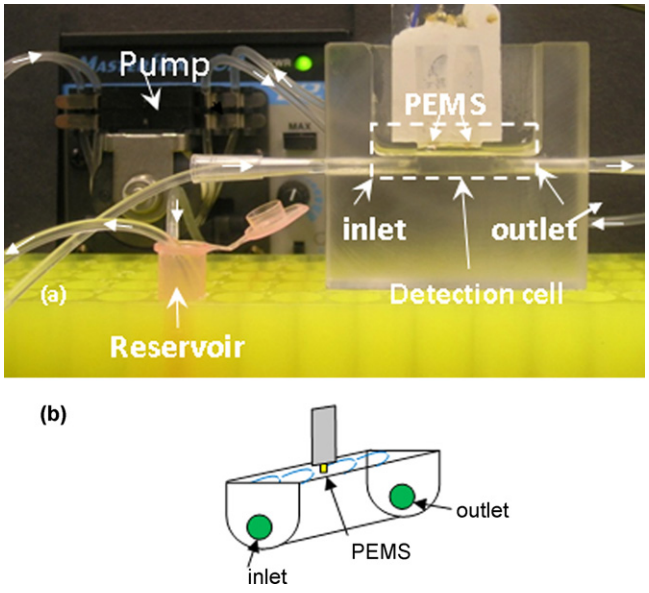

Fig. 2. (a) A photograph of the flow system consisted of an polycarbonate open detection cell indicated by the dashed rectangle, a reservoir (the pink PCR tube), a peristaltic pump connected with tubes of a 1.5 mm inner diameter and (b) a schematic of the detection chamber. Both the inlet and the outlet of the detection cell were located near the bottom of the cell while the PEMS were situated near the top of the detection cell and at the center of the flow cell with the major faces of the PEMS parallel to the flow. Both the inlet and outlet tubes were over 1 m long such that the tubes and the reservoir together accounted for most of the 6 ml of liquid volume. The arrows along the tubing indicate the direction of the flow.

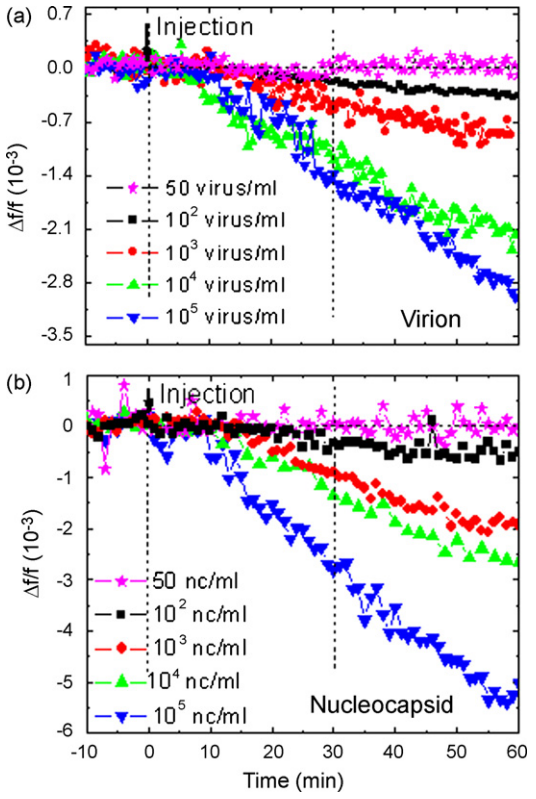

Fig. 3. $\Delta f/f$ versus time for (a) virion detection at various virion concentrations and (b) for nucleocapsid detection at various nucleocapsid concentrations.

According to Shih et al. (2008), the relative resonance frequency shift, $\Delta f/f$, was independent of the length and width of the PEMS and was only proportional to the surface stress, s, resulted from antigen binding and inversely proportional to the thickness, h, of the device as $\Delta f/f \propto s/h$ where f was the initial resonance frequency and Δf the resonance frequency shift defined as the difference of the resonance frequency at time, t, and the initial resonance frequency at $t = 0$. For the same antigen–antibody pair, the surface stress, s, would only depend on the concentration and for the same antigen concentration, s would only depend on the antibody–antigen pair used. As all current PEMS had the same thickness but varying lengths, we plot $\Delta f/f$ versus time for the direct detection of the viruses with anti-VP28 antibody coated PEMS for concentrations ranging from 10^5–50 viruses/ml in Fig. 3(a). The detection $\Delta f/f$ versus time for nucleocapsid detection using anti-VP664 coated PEMS at concentrations 10^5–50 nucleocapsids/ml is plotted in Fig. 3(b).

Note in all the detection events shown in Fig. 3(a) and (b), there was no discernable artificial signal arising from the spiking events. In addition, there was a delay in the onset of detection until about $t = 10$ min. We attributed the delay in detection and the absence of an artificial signal from spiking to the following preventive measures we had taken: (1) by spiking in a reservoir away from the detection channel to minimize the possibility of artificial spiking signal and to allow more time for mixing, (2) by spiking near the top of the reservoir while keeping the opening of the tubes at the bottom of the reservoir and by using a long (>100 cm) tube connecting the reservoir to the inlet of the detection channel to delay the reach of the virions and nucleocapsides to the detection channel, and (3) by keeping the PEMS near the top of the detection channel while the inlet and outlet were at the bottom of the detection chamber (Fig. 2(b)) to further prevent the virions and nucleocapsides from reaching the PEMS before they were well mixed with the liquid.

From Fig. 3(a) and (b), one can see that starting around $t = 10$ min, $\Delta f/f$ decreased with time for a given virion (nucleocapsid) concentration, signaling binding of the virions (nucleocapsids) to the antibody on PEMS surface. For all concentrations larger or equal to 100 virions (nucleocapsids)/ml, the $|\Delta f/f|$ at $t = 60$ min was larger than the noise the fluctuations of the $\Delta f/f$ with time which was about $5–8 \times 10^{-5}$ (corresponding to a Δf of 60–80 Hz) as discussed below. In contrast, at 50 virions (nucleocapsids)/ml the $|\Delta f/f|$ at $t = 60$ min was smaller than the noise, indicating no positive detection of either the virions or nucleocapsids at this concentrations and the concentration sensitivity for both the virions and the nucleocapsids was 100 virions (nucleocapsids)/ml.

In Tables 1 and 2 we listed the values of f, $\Delta f_{30}/f$ and $\Delta f_{60}/f$ at various virion and nucleocapsid concentrations where Δf_{30} and Δf_{60}

Table 1
Detection data of the whole virus particles at concentrations ranging from 10^5 to 50 virus/ml. where f was the initial resonance frequency, Δf_{30} and Δf_{60} were the resonance frequency shift averaged over $t = 29–31$ min and that averaged over $t = 55–60$ min, respectively. Note that for each Δf and $\Delta f/f$, the numbers after the "±" indicated the noise (half bandwidth) of Δf and $\Delta f/f$ with time, respectively.

Virus concentration (virus/ml)	f (kHz)	$-\Delta f_{30}$ (kHz)	$-\Delta f_{60}$ (kHz)	$-\Delta f_{30}/f$ ($\times 10^{-3}$)	$-\Delta f_{60}/f$ ($\times 10^{-3}$)
10^5	660	1.5 ± 0.07	2.6 ± 0.1	2.3 ± 0.1	3.9 ± 0.15
10^4	843	0.94 ± 0.07	1.9 ± 0.1	1.1 ± 0.08	2.25 ± 0.1
10^3	834	0.41 ± 0.07	0.73 ± 0.07	0.5 ± 0.08	0.9 ± 0.08
10^2	774	0.13 ± 0.07	0.28 ± 0.07	0.17 ± 0.08	0.36 ± 0.08
50	788	0 ± 0.07	0 ± 0.07	0 ± 0.08	0 ± 0.08

Table 2
Detection data of the nucleocapsid particles at concentrations ranging from 10^5 to 50 virus/ml where f was the initial resonance frequency, Δf_{30} and Δf_{60} were the resonance frequency shift averaged over t = 29–31 min and that averaged over t = 55–60 min, respectively. Note that for each Δf and $\Delta f/f$, the numbers after the "±" indicated the noise (half bandwidth) of Δf and $\Delta f/f$ with time, respectively.

Nucleocapsid concentration (virions/ml)	f (kHz)	$-\Delta f_{30}$ (kHz)	$-\Delta f_{60}$ (kHz)	$-\Delta f_{30}/f$ ($\times 10^{-3}$)	$-\Delta f_{60}/f$ ($\times 10^{-3}$)
10^5	650	1.6 ± 0. 1	3.4 ± 0.1	2.46 ± 0.15	5.23 ± 0.15
10^4	640	1 ± 0.07	1.7 ± 0.07	1.56 ± 0.1	2.66 ± 0.1
10^3	650	0.41 ± 0.06	1.2 ± 0.07	0.63 ± 0.08	1.85 ± 0.1
10^2	655	0.15 ± 0.06	0.3 ± 0.06	0.23 ± 0.08	0.45 ± 0.08
50	665	0 ± 0.06	0 ± 0.06	0 ± 0.08	0 ± 0.08

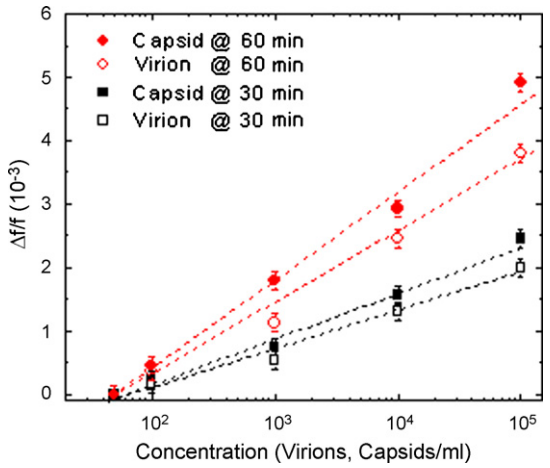

Fig. 4. $\Delta f/f$ versus concentration for virion and nucleocapsid detection at t = 30 and 60 min.

were the resonance frequency shift averaged over t = 29–31 min and that averaged over t = 55–60 min, respectively. Note that for each $\Delta f/f$, the number after the "±" indicated the noise half the band width of the fluctuations of $\Delta f/f$ with time. Although we obtained non-zero values for $\Delta f_{30}/f$ and $\Delta f_{60}/f$ at 50 virions/ml and at 50 nucleocapsids/ml, these values were smaller than the noise of $\Delta f/f$ with time, indicating that they were insignificant. As a result, we recorded zero for the $\Delta f_{30}/f$ and $\Delta f_{60}/f$ for both 50 virions/ml and 50 nucleocapsids/ml in Tables 1 and 2.

To better illustrate the concentration dependence, we plot $\Delta f_{30}/f$ and $\Delta f_{60}/f$ versus concentration for both virions and nucleocapsids in Fig. 4. As can be seen, both $\Delta f_{30}/f$ and $\Delta f_{60}/f$ increased with an increasing concentration for both virion and nucleocapsid. Note that even though both virions and nucleocapsids exhibited a concentration sensitivity of 100 virions/ml, the average frequency shift $\Delta f/f$ was larger for the nucleocapsid than for the virion for every concentration and the difference was larger at t = 60 min than at t = 30 min, indicating that the binding of anti-VP664 to the nucleocapsid was stronger than that of anti-VP28 to the virion. The detailed comparison between the resonance frequency shifts for the virions and those for the nucleocapsids are shown in Table 3. These results compared well with the result of Tsai et al. (2004) where the binding of anti-VP664 to the nucleocapsid and that of the anti-Vp28 to the virion were examined using transmission electron microscopy (TEM). The TEM images showed that there were about 12 anti-VP28 coated gold particles bound to each virion and 21 anti-VP664 coated gold particles to each nucleocapsid indicating that binding of anti-VP664 to a nucleocapsid was stronger than that of anti-Vp28 to a virion, in agreement with the current detection result that at the same concentration, the $\Delta f/f$ for detection of nucleocapsids was higher than that of detection of virions.

Table 3
Comparison of $\Delta f_{60}/f$ between virion detection and nucleocapsid detection.

Virus concentration (virus/ml)	$-\Delta f_{60}/f$ ($\times 10^{-3}$) for virion	$-\Delta f_{60}/f$ ($\times 10^{-3}$) for nucleocapsid
10^5	3.9 ± 0.15	5.23 ± 0.15
10^4	2.2 ± 0.1	2.7 ± 0.11
10^3	0.9 ± 0.1	1.85 ± 0.1
10^2	0.36 ± 0.06	0.45 ± 0.06
50	0 ± 0.05	0 ± 0.075

Note that although we injected a more concentrated suspension (e.g., 1×10^5 virions or nucleocapsids/ml) into a reservoir as a convenient way to achieve a sample of a desired concentration (e.g., 100 virions or nucleocapsids per ml) for detection in the current flow setup it does not imply that PEMS detection would always require injection of a more concentrated liquid in order to achieve positive detection. For example, detection without spiking can be accomplished by using two reservoirs instead of one: one containing the sample and the other PBS. Connection of detection cell to either the sample or to PBS is controlled by the valves. Such a flow system is commonly used in a BIAcore system or a quartz crystal microbalance (QCM). In a future study, we will examine PEMS detection with such a flow system. However, design and implementation of such of a flow system is not within the scope of this study.

The current flow rate of 1 ml/min corresponded to a flow velocity of u = 1.4 mm/s, which could be further increased to potentially increase the detection signal (McGovern et al., 2008). This is because an increase of flow velocity could circulate a larger liquid volume thus bringing more virions/nucleocapsids to pass the sensor surface per unit time, thereby increasing the chance for the virions and nucleocapsids to bind to the sensor surface. On the other hand, an increase in flow rate can also increase the force impinging on a bound virion or ncleocapsid on the sensor surface leading to detachment of the bound virions/nucleocapsids and potentially lead to decrease of detection signal. The flow induced impingement force can be estimated as $F = 1.7(6\pi\eta a)u$ (McGovern et al., 2008) where η = 1 cP is the liquid viscosity, a the radius of the virion or nucleocapsid. As the largest dimension of either the virion or the nucleocapsid is on the order of 300 nm, we use a = 150 as an overestimate and the impingement force for the bound virions or nucleocapsids at a flow velocity of 1.4 mm/s was estimated to be about 6 pN, which was still quite small compared to the 100 pN shown to unbind particles from the sensor surface that were bound by antibody–antigen binding (McGovern et al., 2008). Based on this estimation, it is, therefore, likely that one can further increase detection signal and lower detection concentration limit by increasing the flow velocity, which will be examined in a future study and is not within the scope of the present study.

4. Conclusion

We have investigated rapid, label free detection of WSSV virions and nucleocapsids using the first longitudinal extension resonance peaks of 5 PMN–PT/Cu PEMS 1050–700 μm long and 850–485 μm wide. The PMN–PT/Cu PEMS were consisting of an 8 μm thick PMN–PT layer bonded with a 2 μm thick copper and further elec-

trically insulated with a MPS coating. Detection of the virions and nucleocapsids was carried out by directly inserting the anti-VP28 and anti-VP664 coated PEMS at the center of the detection cell. The flowing suspension of 10^5–50 virions (nucleocapsids)/ml was created through a 100-fold dilution by spiking 60 μl of a 100-time concentrated suspension in a reservoir away from the detection channel to minimize the artificial spiking signal and prevent the PEMS from unwanted exposures to the un-mixed concentrate. Label free detection of virions and nucleocapsids was achieved by monitoring the PEMS resonance frequency shift with time. We showed that both the virions and the nucleocapsids could be detected at a concentration 100 virions (nucleocapsids)/ml or 10 virions (nucleocapsids)/100 μl, comparable to the detection sensitivity of PCR. However, in contrast to PCR, PEMS detection was label free, in situ, and rapid (less than 30 min), potentially requiring minimal or no sample preparation.

Acknowledgments

This work is supported in part by the National Institute of Health (NIH) under grant no. R01 EB000720, and The Nanotechnology Institute, a University Grant program of the Commonwealth of Pennsylvania's Ben Franklin Technology Development Authority through Ben Franklin Technology Partners of Southeast Pennsylvania.

References

Anil, T.M., Shankar, K.M., Mohan, C.V., 2002. Dis. Aquat. Org. 51 (1), 67–75.
Capobianco, J.A., Shih, W.Y., Shih, W.-H., 2006. Rev. Sci. Instrum. 77 (12), 125105.
Capobianco, J.A., Shih, W.Y., Shih, W.-H., 2007. Rev. Sci. Instrum. 78 (4), 046106.
Capobianco, J.A., Shih, W.Y., Yuan, Q.-A., Adams, G.P., Shih, W.-H., 2008. Rev. Sci. Instrum. 79 (7), 076101.
Capobianco, J., 2009, Ph.D. Thesis. Drexel University, Philadelphia, PA 10104.
Chang, P.S., Lo, C.F., Wang, Y.C., Kou, G.H., 1996. Dis. Aquat. Org. 27 (2), 131–139.
Chen, G.Y., Thundat, T., Wachter, E.A., Warmack, R.J., 1995. J. Appl. Phys. 77 (8), 3618–3622.
Corbel, V., Zuprizal, Shi, Z., Huang, C., Sumartono, Arcier, J.M., Bonami, J.R., 2001. J. Fish Dis. 24 (7), 377–382.
Chou, H.Y., Huang, C.Y., Wang, C.H., Chiang, H.C., Lo, C.F., 1995. Dis. Aquat. Org. 23 (3), 165–173.
Durand, S., Lightner, D.V., Nunan, L.M., Redman, R.M., Mari, J., Monami, J.R., 1996. Dis. Aquat. Org. 27 (1), 59–66.
Durand, S.V., Lightner, D.V., 2002. J. Fish Dis. 25 (7), 381–389.
Sritunyalucksana, K., Srisala, J., McColl, K., Nielsen, L., Flegel, T.W., 2006. Aquaculture 255 (1–4), 95–104.
Flegel, T.W., 2006. Aquaculture 258 (1–4), 1–33.
Gupta, A.K., Nair, P.R., Akin, D., Ladisch, M.R., Broyles, S., Alam, M.A., Bashir, R., 2006. PNAS 103 (36), 13362–13367.
Hwang, K.S., Lee, J.H., Park, J., Yoon, D.S., Park, J.H., Kim, T.S., 2004. Lab. Chip 4 (6), 547–552.
Kimura, T., Yamano, K., Nakano, H., Momoyama, K., Hiraoka, M., Inouye, K., 1996. Fish Pathol. 31 (2), 93–98.
Lightner, D.V. (Ed.), 1996. A handbook of pathology and diagnostic procedures for diseases of penaeid shrimp. World Aquaculture Society, Baton Rouge, LA, USA, 305 pp.
Lee, J.H., Hwang, K.S., Park, J., Yoon, K.H., Yoon, D.S., Kim, T.S., 2005. Biosens. Bioelectron. 20, 2157–2162.
Lee, J.H., Kim, T.S., Yoon, K.H., 2004a. Appl. Phys. Lett. 84 (16), 3187–3189.
Lee, J.H., Yoon, K.H., Hwang, K.S., Park, J., Ahn, S., Kim, T.S., 2004b. Biosens. Bioelectron. 20, 269–275.
Lei, Y., Chen, H., Dai, H., Zeng, Z., Lin, Y., Zhou, F., Pang, D., 2008. Biosens Bioelectron. 23 (7), 1200–1207.
Liu, W., Wang, Y.T., Tian, D.S., Yin, Z.C., Kwang, J., 2002. Dis. Aquat. Org. 49 (1), 11–18.
Lo, C.F., Ho, C.H., Peng, S.E., Chen, C.H., Hsu, H.C., Chiu, Y.L., Chang, C.F., Liu, K.F., Su, M.S., Wang, C.H., Kou, G.H., 1996a. Dis. Aquat. Org. 27 (3), 215–225.
Lo, C.F., Leu, J.H., Ho, C.H., Chen, C.H., Peng, S.E., Chen, Y.T., Chou, C.M., Yeh, P.Y., Huang, C.J., Chou, H.Y., Wang, C.H., Kou, G.H., 1996b. Dis. Aquat. Org. 25 (1–2), 133–141.
McGovern, J.-P., Shih, W.Y., Rest, R., Purohit, M., Pandya, Y., Shih, W.-H., 2008. Analyst 133 (5), 649–654.
McGovern, J.P., Shih, W.Y., Shih, W.-H., 2007. Analyst 132 (8), 777–783.
Okumura, T., Nagai, F., Yamamoto, S., Oomura, H., Inouye, K., Ito, M., Sawada, H., 2005. J. Virol. Meth. 124 (1–2), 143–148.
Poulos, B.T., Pantoja, C.R., Bradley-Dunlop, D., Aguilar, J., Lightner, D.V., 2001. Dis. Aquat. Org. 47 (1), 13–23.
Sakti, S.P., Rosler, S., Lucklum, R., Hauptmann, P., Buhling, F., Ansorge, S., 1999. Sens. Actuator A: Phys. 76 (1–3), 98–102.
Shen, Z., Shih, W.Y., Shih, W.-H., 2006. Appl. Phys. Lett. 89, 023506–23508.
Shih, W.Y., Luo, H., Li, H., Martorano, C., Shih, W.H., 2006. Appl. Phys. Lett. 89, 242913.
Shih, W.Y., Zhu, Q., Shih, W.-H., 2008. J. Appl. Phys. 104, 074503.
Takahashi, Y., Itami, T., Maeda, M., Suzuki, N., Kasornchandra, J., Supamattaya, K., Khongpradit, R., Boonyaratpalin, S., Kondo, M., Kawai, K., Kusuda, R., Hirono, I., Aoki, T., 1996. J. Fish Dis. 19 (5), 399–403.
Tremont, R., De Jesus-Cardona, H., Garcia-Orozco, J., Castro, R.J., Cabrera, C.R., 2000. J. Appl. Electrochem. 30 (6), 737–743.
Tsai, J.M., Wang, H.C., Leu, J.H., Hsiao, H.H., Wang, A.H., Kou, G.H., Lo, C.F., 2004. J. Virol. 78 (20), 11360–11370.
Wang, C.H., Lo, C.F., Leu, J.H., Chou, C.M., Yeh, P.Y., Chou, H.Y., Tung, M.C., Chang, C.F., Su, M.S., Kou, G.H., 1995. Dis. Aquat. Org. 23 (3), 239–242.
Wang, C.S., Tang, K.F.J., Kou, G.H., Chen, S.N., 1997. J. Fish Dis. 20 (5), 323–331.
Wang, Y.C., Lo, C.F., Chang, P.S., Kou, G.H., 1998. Aquaculture 164 (1–4), 221–231.
Wang, H.C., Wang, H.C., Leu, J.H., Kou, G.H., Wang, A.H., Lo, C.F., 2007. Dev. Comp. Immunol. 32 (7), 672–686.
Wongteerasupaya, C., Vickers, J.E., Sriuairatana, S., Nash, G.L., Akarajamorn, A., Boonsaeng, V., Panyim, S., Tassanakajon, A., Withyachumnarnkul, B., Flegel, T.W., 1995. Dis. Aquat. Org. 21 (1), 9–77.
Wongteerasupaya, C., Wongwisansri, S., Boonsaeng, V., Panyim, S., Pratanpipat, P., Nash, G.L., Withyachumnarnkul, B., Flegel, T.W., 1996. Aquaculture 143 (1), 23–32.
Xie, X., Li, H., Xu, L., Yang, F., 2005. Virus Res. 108 (1–2), 63–67.
Yi, J.W., Shih, W.Y., Shih, W.-H., 2002. J. Appl. Phys. 91 (3), 1680–1686.
Yi, J.W, Shih, W.Y., Shih, W.-H., Mutharasan, R., 2003. J. Appl. Phys. 93, 619–625.
Zhou, Q., Qi, Y.P., Yang, F., 2007. J. Virol. Meth. 146 (1–2), 288–292.
Zhu, Q., Shih, W.Y., Shih, W.H., 2007a. Biosens. Bioelectron. 22 (12), 3132–3138.
Zhu, Q., Shih, W.Y., Shih, W.H., 2007b. Sens. Actuator B: Chem. 125 (2), 379–388.
Zhu, Q., Shih, W.Y., Shih, W.-H., 2008a. Appl. Phys. Lett. 92, 033503.
Zhu, Q., Shih, W.Y., Shih, W.-H., 2008b. Appl. Phys. Lett. 92, 183505–183507.